13

Effect of substrate temperature on the morphology and photoelectric properties of thin films of the molecular semiconductor subphthalocyanine boron chloride

© K.M. Gordeev, A.I. Koptyaev, G.L. Pakhomov

Institute of Physics of Microstructures, Russian Academy of Sciences,
Nizhny Novgorod, Russia
e-mail: kgor@ipmras.ru

Received August 1, 2025
Revised November 5, 2025
Accepted November 7, 2025

The microscopic morphology of thin layers of a low-molecular semiconductor, subphthalocyanine boron chloride (SubPC) is known to undergo substantial changes with increasing substrate temperature during vacuum deposition. In this work, the deposition temperature range was extended toward lower temperatures, from 70 °C to −35 °C. Optical and X-ray studies, along with morphological data of the films, revealed indications of an anomalous growth mechanism transition. Presumably, this is due to thermally activated migration of the molecular aggregates composed of two SubPc molecules (dimers), which have a higher affinity for the substrate surface than single molecule (monomers). Multilayer photodiodes with a molecular heterojunction *p*-SubPc/*n*-C_{60} were fabricated, where SubPc layer was deposited at different temperatures. The best sample with rectification of $\sim 9 \cdot 10^3$ and photo-to-dark current ratio of $\sim 3 \cdot 10^4$ was obtained with the SubPc layer deposited at a substrate temperature of 0 °C, thus having rather crystalline structure.

Keywords: molecular semiconductors, thin films, growth mechanism, thermodynamic control, photodiode performance.

DOI: 10.61011/TP.2026.03.63170.203-25

Introduction

Optoelectronic devices based on small organic molecules are of interest when solving such problems as spectral range extension or reduction of device weight, non-invasive medical diagnosis [1–4], space exploration, etc. Compared with polymers, small organic molecules with a cyclic system of π-conjugated bonds are of interest due to their photoactivity, ability to select an absorbed/emitted light wavelength range and a component manufacturing technique.

New compounds are regularly synthesized to find a more favorable molecular structure for optoelectronic applications. But this doesn't mean that the potential of already known molecules has been exhausted. Firstly, they are usually more readily available and have predictable performance. Secondly, the key properties of a device that define its efficiency such as charge carrier mobility and exciton diffusion length depend on intermolecular processes within the condensed phase sometimes in a greater extent than on the intramolecular structure [5]. Widely known low-molecular semiconductors, phthalocyanine and related compounds, pentacene, and fullerenes suit perfectly the device manufacturing process because they are thermally stable and can be deposited via physical vapor deposition (PVD) in the form of uniform coatings [1,3–22]. Moreover, thin film morphology, including the phase composition and surface relief, depend on substrate affinity of molecules and on thickness, or is modified *ex situ* via annealing [22]. Morphology tuning for a particular device allows many-fold increase in device output parameters [1,4,6,8,10,12,17,18,20].

Adherence to particular PVD process conditions using deposition rate (kinetic control) or substrate temperature T_g (thermodynamic control) is the most technologically-reasonable method of such tuning [6,8–10,12,23]. For anisotropic planar or conical molecules, for example, transition metal phthalocyanines, the higher the substrate temperature and the slower the deposition rate are, the higher the film crystallinity and roughness are, up to the uniformity loss and growth of individual single crystals [7]. However, for boron chloride subphthalocyanine (SubPc), the literature describes a more complex dependence of the molecular packing on deposition rate and T_g [8,12]. SubPc is a promising material for hybrid thin-film optoelectronic devices [1,4,8,12,15–18]. Theoretical description of growth processes can be more elaborate in cases when not only monomer, but also dimer and trimer are capable of diffusion along the substrate surface [9,23].

For better understanding of the substrate temperature on morphology and conductivity of SubPc layers obtained via the PVD process, growth at different T_g was used in this work. It was detected that, unlike phthalocyanines, substrate heating actually led to loss of crystallinity detected by standard X-ray techniques, reduction of roughness and step-by-step transition from nonuniform island-type morphology to more uniform and homogeneous one.

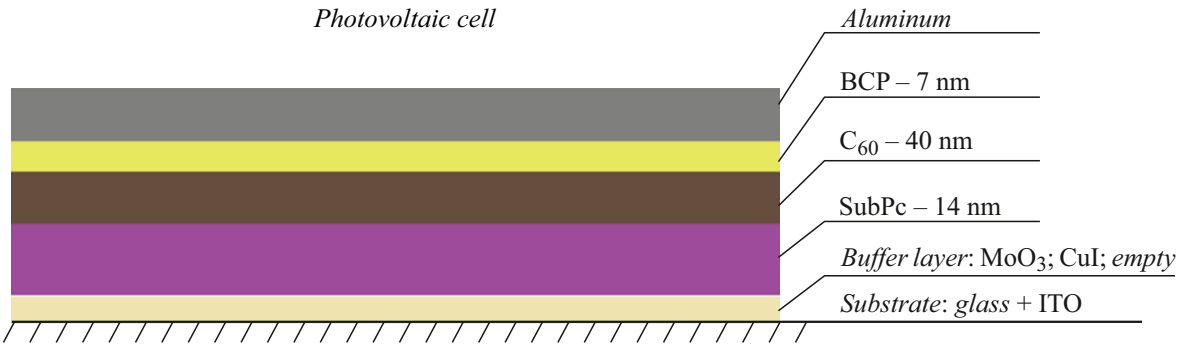

Figure 1. Diagram of a multilayer cell with an n-type SubPc layer.

1. Experiment

This study used commercial reagents (Merck): boron chloride subphthalocyanine (SubPc), fullerene C_{60}, bathocuproine (BCP), molybdenum oxide MoO_3.

Silicon wafers (100), glasses coated with double indium-tin oxide (ITO), amorphous quartz with lithographically patterned golden interdigital electrodes with a gap of 30 μm, height of 150 nm and total channel length of 105.8 mm were subjected to ultrasonic cleaning with acetone and isopropyl alcohol and to drying in high purity argon flow.

Vacuum deposition of model SubPc and C_{60} photoabsorber layers, buffer layers and top aluminum electrode for thin-film device prototypes was carried out using the modernized VUP-5M system with a residual pressure not higher than 10^{-4} Pa with a self-made additional module for substrate temperature T_g control within $-35\,^\circ\mathrm{C} - 70\,^\circ\mathrm{C}$ [7] and thickness control using a quartz crystal microbalance (QCM).

Surface relief, optical spectra, crystal structure and electric properties were studied using atomic force microscopy (AFM) (CMM 2000, Proton-MIET) and white light interferometry (WLI) (TalySurf CCI 2000), Genesys-50 spectrophotometer (ThermoScientific), D8 Discover Bruker X-ray diffractometer, and Keithley 4200-SCS curve tracer, respectively. Slow deposition rate for SubPc < 0.03 nm/s was chosen to minimize the effect of kinetic aspects on film growth [8]. For multilayer structures on ITO substrates, thickness is reduced to (14 ± 1) nm to make it closer to the best values known from the literature [12,24]. Device prototypes were made using the following scheme: ITO/buffer layer/SubPc 14 nm/C_{60} 40 nm/BCP 8 nm/Al 80 nm, where the buffer layer is either 5 nm MoO_x or 7 nm CuI, or none (Figure 1).

2. Results

Nominal thickness of SubPc films deposited onto silicon wafers for AFM relief analysis (Figure 2) was equal to 30 nm as measured using the X-ray reflectometry and WLI on 40 °C and 70 °C films. Measurement of film thickness at lower T_g becomes inaccurate due to too high roughness (Table 1, Figure 3), but for film deposition according to QCM absolutely the same amount of substance by weight was used. Height difference on the AFM map is 3 to 26 times larger than the nominal thickness (Figure 2), and the lower the growth temperature, the higher the height difference.

The observed relief can be divided into three types in accordance with the growth pattern: islands with empty gaps ($-35\,^\circ\mathrm{C} - 0\,^\circ\mathrm{C}$), filled surface with pronounced islands ($20\,^\circ\mathrm{C}$–$40\,^\circ\mathrm{C}$), virtually homogenous surface ($70\,^\circ\mathrm{C}$). Basically, all three types were observed earlier during phthalocyanine film growth [25,26], but never on the same material and the same growth surface simultaneously. Advantage of the chosen T_g range is also in that it can be provided by an additional module with Peltier elements, which is simple in design [7]. AFM images of SubPc ultrathin layers, where the weight of the deposited substance was 20 times lower than that of the layer with $H = 30$ nm, indicate that SubPc nuclei with different shapes, sizes and packing density depending on T_g were formed on the silicon surface (Figure 4). AFM images of films deposited via substrate heating (Figure 2, *d*,*f*) contain maximum one center of growth on the field width of 4.5 μm, the distance between nuclei is 10–20 μm (Figure 5). Even from the analysis of AFM in Figure 2 it becomes apparent that the picture of substrate surface filling with organic material after nucleation changes noticeably with temperature as if their affinity γ^* has changed (see equation (1)): from growth mainly on nuclei at $T_g \leq 0\,^\circ\mathrm{C}$ to growth mainly on the surface at $T_g \geq 40\,^\circ\mathrm{C}$. Unfortunately, AFM resolution in semi-contact mode is insufficient to detect accurately whether a wetting layer is present or absent on the surface (in contact mode, the cantilever tip mechanically breaks the organic layer), this does not allow one to make a precise conclusion on the film growth mechanisms.

The applicability problem of classical growth models is in that they were initially built for epitaxy of covalent-bonded inorganic crystal films [23]. In the most general terms, interaction is described by equation [9]:

$$\gamma_s = \gamma^* + \gamma_d \cos\theta, \qquad (1)$$

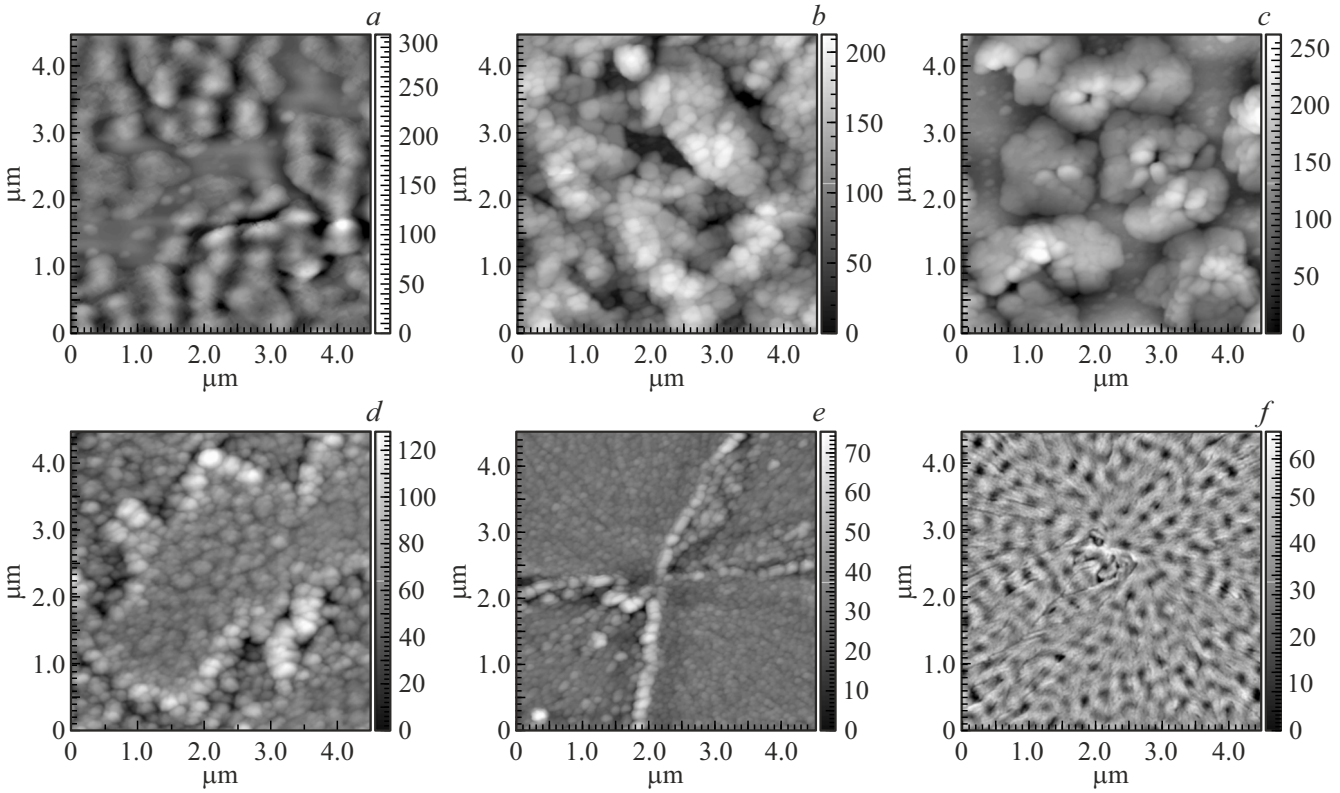

Figure 2. AFM surface relief of SubPc films deposited at the following substrate temperatures: *a* — −35 °C, *b* — −20 °C, *c* — 0 °C, *d* — 20 °C, *e* — 40 °C, *f* — 70 °C.

Table 1. AFM surface relief analysis data for SubPc films on silicon. Calculation was performed for $9 \times 9\,\mu$m frames

Tg, °C	RMS, nm	A/H^*	S/S_{LF}^{**}, %
−35	107.7	26	20
−20	43.9	10	8
0	52.8	13	23
20	16.8	5.2	0
40	7.0	3.8	0
70	9.7	3	0

Note. $^*A/H$ — ratio of relief amplitude to nominal thickness of the SubPc layer $H = 30$ nm; $^{**}S/S_{\mathrm{LF}}$ — proportion of substrate area with low material filling level.

where γ_s is the substrate surface energy, γ^* is the molecule-substrate interface energy, γ_d is the deposited material surface energy, surface energy = surface tension in earlier sources [23], θ is the contact angle between the substrate surface and the tangent to nucleus in the triple line.

Despite its low applicability to the vacuum growth of molecular films, this equation correctly reflects the morphology control philosophy, for a drastic change in the growth mechanism either γ_s or γ_d shall be changed or their affinity γ_* shall be affected. However, a narrow range of T_g away from the SubPc sublimation temperature (250 °C) chosen for the study doesn't imply that the thermodynamically equilibrium growth is achieved.

For organic crystal phases formed due to Van der Waals forces, the molecule-surface interaction energy is not always rigidly determined. This is due to the fact that molecules have a much larger volume and a complex shape, i.e. are anisotropic in themselves. For them and especially for their aggregates, substrate affinity can vary significantly depending on orientation with respect to the growth surface. In particular, a SubPc molecule can be described as a three-sided pyramid with a base width of 11.9 Å and a height of 4.2 Å and taking into account the Van der Waals radii (≈ 1.5 Å) — about 15 Å and 7 Å respectively. Maximum dimension of a binary aggregate, according to the CCDC 2363922 X-ray diffraction analysis data [18], will be 20.3 Å. Phthalocyanine and porphyrin molecules porphyrin related to SubPc on many technical (not specially prepared) substrates prefer to „tiptoe" when molecule planes are oriented vertically or inclined at an angle to the substrate [10,27]. SubPc is no exception, diffraction patterns of films contain signals at 20.7 and 22°, reflections from planes (221) and (122), where the molecule is inclined with respect to the substrate at 65.67° and 39.37°, respectively [12]. Similar molecule angles 45° and 74° in films occur in zinc phthalocyanine [11,27].

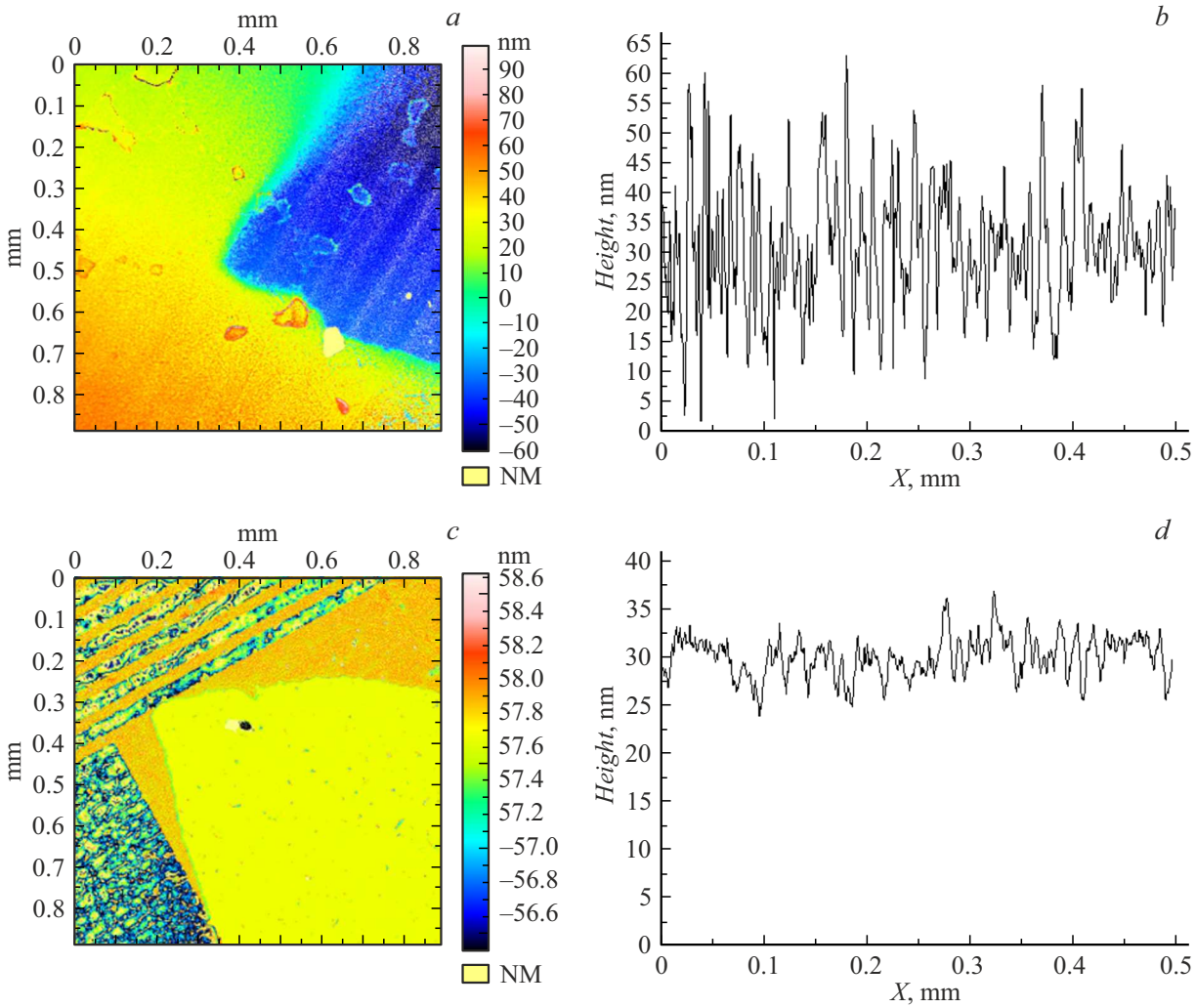

Figure 3. Thickness and relief measurement by white light interferometry (WLI). Surface relief maps of SubPc films made at $T_g = -35\,^{\circ}\mathrm{C}$ on the quartz surface (a) and at $T_g = 70\,^{\circ}\mathrm{C}$ on the surface of substrates with interdigital electrodes (b). Low relief pads were shaded by substrate fixtures during sputtering; c, d — surface profiles of the corresponding films.

Growth scenarios for layers with orientation of Pc or SubPc molecules parallel to the substrate are also known, this happens when molecules are deposited onto a surface-active layer, for example, Cu(111) [14,28] or CuI [13], i.e. due to an increase in γ_s. In the case when, for example, single-crystal metal is deposited on the surface, the molecule-surface interaction force is such that inherently cone-shaped SubPc macrocycle is flattened [14], spherical C_{60} molecules are also susceptible to transformation [22]. Applying a high-power electric field to the deposition zone is another molecule reorientation option [15]. SubPc molecules have a permanent dipole moment (PDM) directed vertically from the macrocycle reference plane to the Cl atom, which is estimated as 5.5 D [29]. Orientation interaction between polar molecules, a so-called Keesom dipole-dipole effect, is the strongest of three classical types of Van der Waals bond. Consequently, it also defines the molecule packing method within a crystal and thin layer anisotropy [1]. PDM becomes particularly important for discussing molecular layer polarization and local transformation processes when potential is applied in running devices. Therefore in [15], molecules are packed during deposition into a textured film, orienting parallel to the substrate, and the X-ray diffraction pattern contains a typical signal 17.01° of reflection from plane (002). We also observe a similar, but very weak signal in diffraction patterns of SubPc films deposited at $-35\,^{\circ}\mathrm{C}$–$20\,^{\circ}\mathrm{C}$ (Figure 6, a). It indicates that at low temperatures in nucleus crystallites formed on the silicon wafer, molecules are placed parallel to the substrate (Figure 6, b, c). Thermodynamic restrictions are imposed on the nucleus packing density (N_{D}) and maximum area of crystal faces (ΣA_i) [9]: the lower the temperature is, the higher the density is, but the smaller the limit crystallite size is (Figure 2, 4, 5). It should be emphasized that it is not possible to identify a direct impact of any kinetic restriction, for example, diffusion length [23] on the layer uniformity

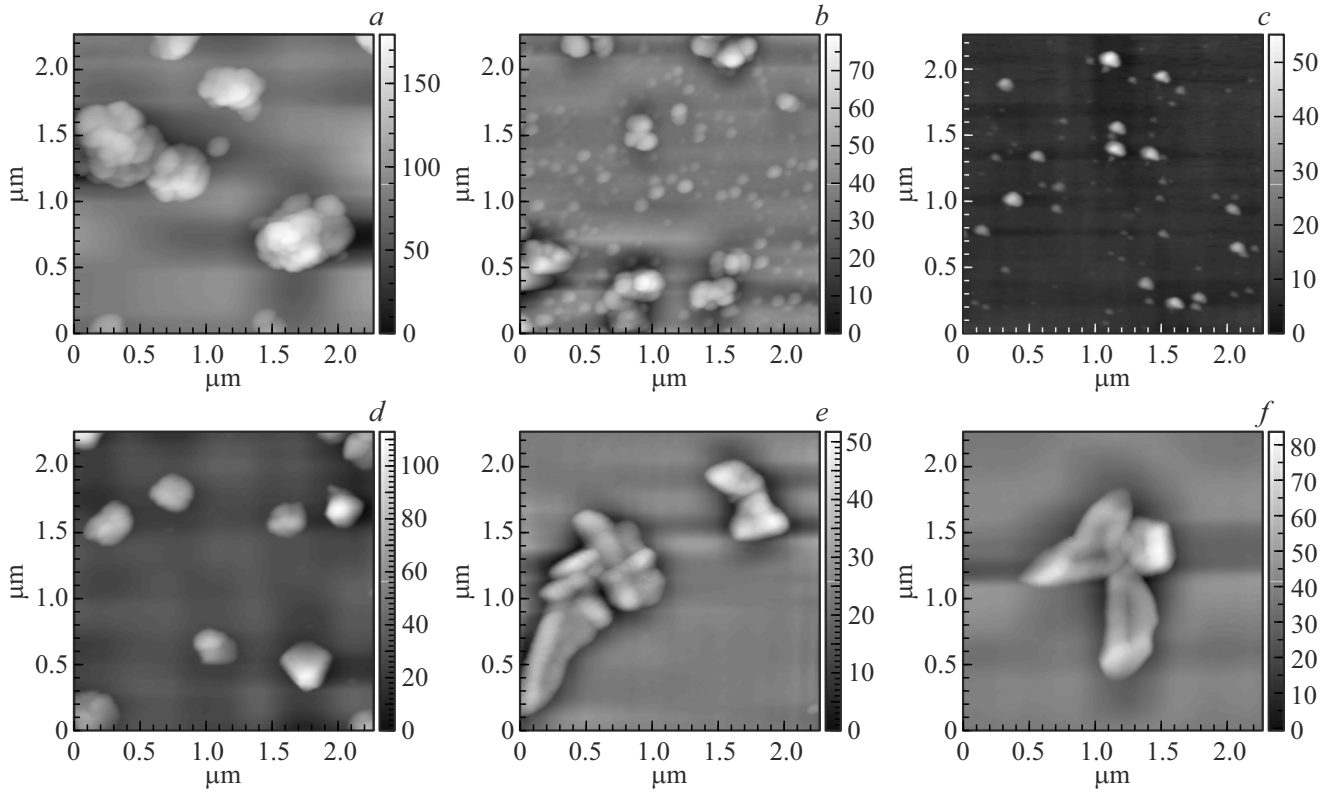

Figure 4. AFM of SubPc ultrathin films fabricated by deposition of 5 % of the boron chloride subphthalocyanine weight taken for films with a nominal thickness of 30 nm at the following substrate temperatures: *a* — −35 °C, *b* — −20 °C, *c* — 0 °C, *d* — 20 °C, *e* — 40 °C, *f* — 70 °C.

and crystallinity in the studied temperature range: even at $T_g - 35\,^\circ$C, the time of free molecule existence on the surface (τ_s) turns out to be sufficient to cover a distance of at least 250 nm, due to which there are unfilled gaps on the substrate (Figure 2, Table 1).

As mentioned above, AFM images of $-35\,^\circ$C$-0\,^\circ$C films contain pure substrate areas (Figure 2, *a*–*c*). After filling the substrate surface with SubPc islands, the growth of new crystals starts from free nucleus faces and is directed in such a way as to avoid the substrate contact as far as possible. As a result, island morphology of films is retained at long distances from the surface and is caused by only intermolecular interaction forces and thermodynamic grain size control [9].

At $T_g = 0\,^\circ$C, the film has the most unique structure (Figure 2, *c*). Its relief consists of high islands with a hole in the center. In the horizontal cross-section, many of these islands have a form of a Reuleaux triangle (width about 1.7 μm at the base). We suppose that such structures are formed in several steps. Step 1 - truncated triangular pyramids similar to those shown in [15] grow on the nucleation centers to some thermodynamically-driven limit size. It is them which provide the 17.01° signal in X-ray images and, therefore, molecules in such crystallites are parallel to the substrate. Step 2 - three formed side faces of a truncated pyramid achieve such area that they become most active secondary nucleation centers, therefore further growth of clusters is directed vertically upwards from them. Horizontal nucleus surface remains unfilled because it is less attractive for aggregation of SubPc molecules, and a hole is formed in the center of the island. Step 3 - molecules adsorbed on the substrate and vertices of truncated pyramids have no enough free path time τ_s to reach the vertex of the growing triangular column and they adhere to the column sides, rounding the island cross-section to a Reuleaux triangle. This is the picture at 0 °C that gave us an idea that the growth of SubPc molecule clusters likely had temperature-dependent priority directions. At low temperatures, a cluster predominantly grows in direction of crystal axes *a* and *b*, first forming a face along plane (002), which is connected to the substrate (Figure 6, *b*, *c*). Growth along the *c* axis, i.e. vertically, is highly hindered due to the complex pyramidal packing (Figure 6, *b*, *c*, Figure 7).

As shown in Figure 7, SubPc molecules are arranged in pairs in the crystal. In [30], quantum chemical calculations were performed for orbital energies and absorption spectra in the region of *Q*-band for 12 possible relative molecular orientations of SubPc dimers selected from the crystal structure, only five of which turned out to be distinguishable by energies. Only one option, dimer 1, with „convex-to-convex“ type orientation gives a bathochromic shift of the principal absorption band relative to the SubPc

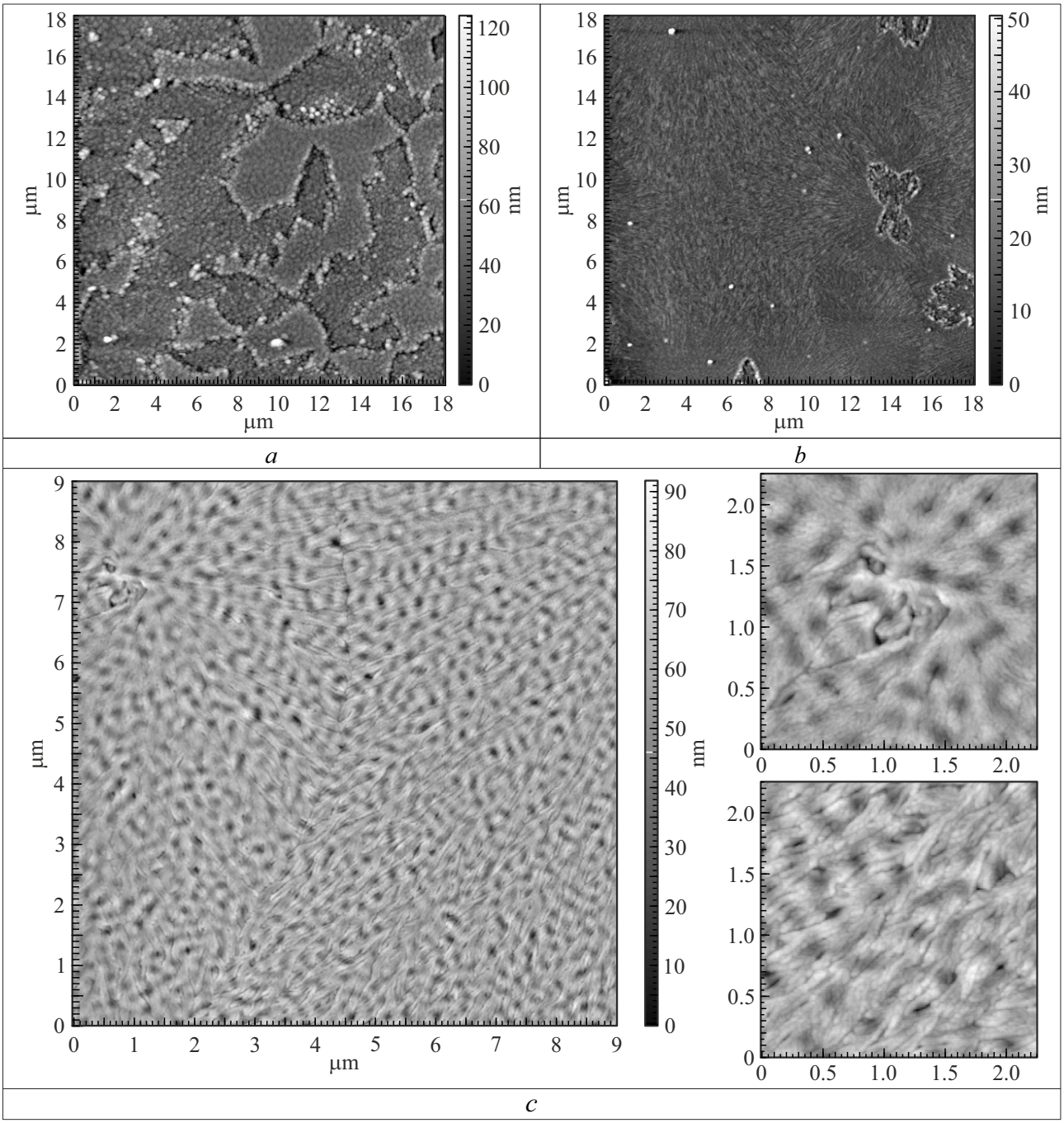

Figure 5. AFM images of SubPc films with a nominal thickness of 30 nm deposited at the following substrate temperatures: *a* — 20 °C, *b* — 40 °C, *c* — 70 °C.

monomer spectrum, and dimer 2 with the „concave-to-concave“ orientation is the most stable in terms of the bond energy [30]. In different translations of the SubPc crystal lattice cell, proportions of type 1 and 2 dimers will be different. For clarity, axes of the„convex-to-convex“ and „concave-to-concave“ type dimer aggregates are marked in Figure 7 with blue and red lines, respectively. Then, crystals formed at low T_g predominantly contain dimers 1, and the ratio of dimers 1 and 2 is controlled thermodynamically.

Electronic absorption spectra shown in Figure 8 confirm this assumption. In organic solutions, SubPc molecules are not prone to aggregation [1], therefore the given spectrum in toluene characterizes light absorption by monomer molecules. It contains two bands — *B*-band with its maximum at 305 nm and *Q*-band with its maximum at 565 nm responsible for electronic transitions between molecular orbitals HOMO-1 → LUMO and HOMO → LUMO (highest occupied and lowest unoccupied molecular orbitals) [1,31].

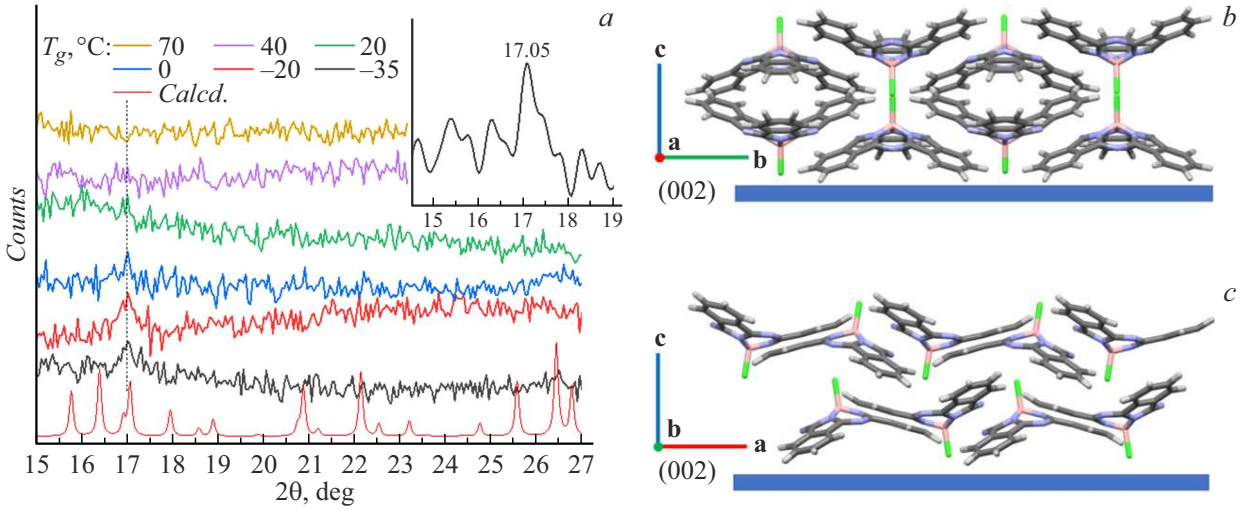

Figure 6. *a* — X-ray diffraction patterns of SubPc films deposited on silicon (100) at various temperatures compared with a diffraction pattern calculated (Calcd) from the CCDC 123269 X-ray diffraction analysis data; inset — result of FFT processing of film diffraction pattern at $T_g = -35\,^{\circ}$C; *b*, *c* — SubPc molecule packing in crystals and orientation with respect to plane (002) in the projection of vectors **bc** (*b*) and **ac** (*c*).

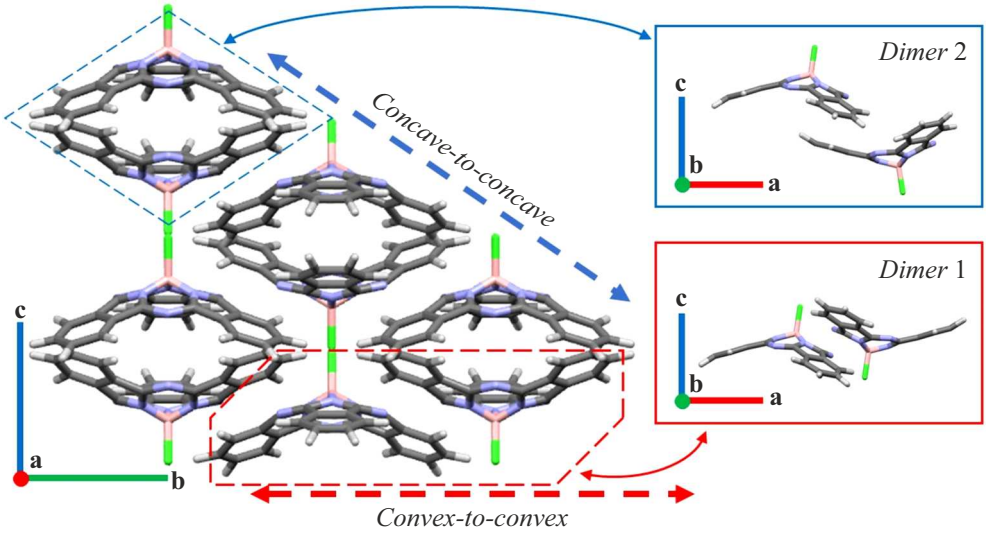

Figure 7. Position of molecules in the SubPc crystallite in the projection of vectors **cb** simulated on the basis of the CCDC 123269 X-ray diffraction analysis data. The packing scheme doesn't contradict the CCDC 2363922 X-ray diffraction data updated by Zigelstein et al. [18]. Insets show relative positions of molecules in type 1 and 2 dimer aggregates in the projection of vectors **ac**.

Since the SubPc molecule is curved and has a low symmetry [1], calculated HOMO for resonance π-conjugated systems, i.e. molecular orbitals $2a_1$ and $2a_2$ are not identical in energy [31]. *Q*-band contains two absorption peaks (Figure 8) corresponding to electronic transitions from these orbitals to a common LUMO: $2a_1 \rightarrow 1e^*$ provides the base maximum, $2a_2 \rightarrow 1e^*$ in the spectrum has a form of a short-wavelength arm [31].

Absorption peaks in SubPc film spectra (Figure 8) relative to toluene solution are shifted bathochromically by $30 - 40$ nm, which corresponds to a larger proportion of dimers 1. This shift is larger by 8 nm than that of film deposited at $-35\,^{\circ}$C relative to the spectra of films deposited at $20\,^{\circ}$C. At $T_g = 70\,^{\circ}$C, the *Q*-band maximum is not shifted relative to $T_g = 20\,^{\circ}$C, but absorption intensity at a wavelength shorter than 550 nm is much higher. Intensity at 550 nm in the spectrum of film deposited at $0\,^{\circ}$C is a little lower than at $20\,^{\circ}$C, but higher than at $-35\,^{\circ}$C, and the base peak retains its position as at $20\,^{\circ}\text{C} - 70\,^{\circ}$C. Besides the gradual intensity growth, spectra deconvolution has detected a hypsochromic shift of a submaximum at 550 nm with increasing T_g. According to quantum chemical calculations [30], it is responsible for transition to the „third $\pi \rightarrow \pi^*$ excited state" of SubPc dimers. This is due to

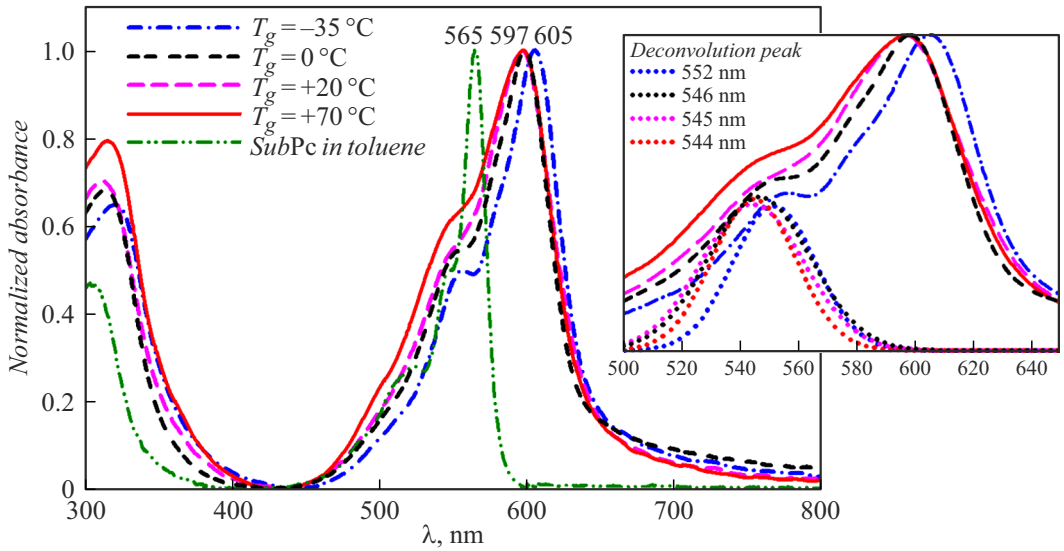

Figure 8. Electronic absorption spectra of SubPc films on a transparent quartz substrate deposited at different temperatures compared with a spectrum of molecules in toluene solution. Inset — position of absorption submaximum at 550 nm clarified using deconvolution. Spectra are normalized to the principal maximum of Q-band ($\lambda = 597 - 605$ nm for films, $\lambda = 565$ nm for solution).

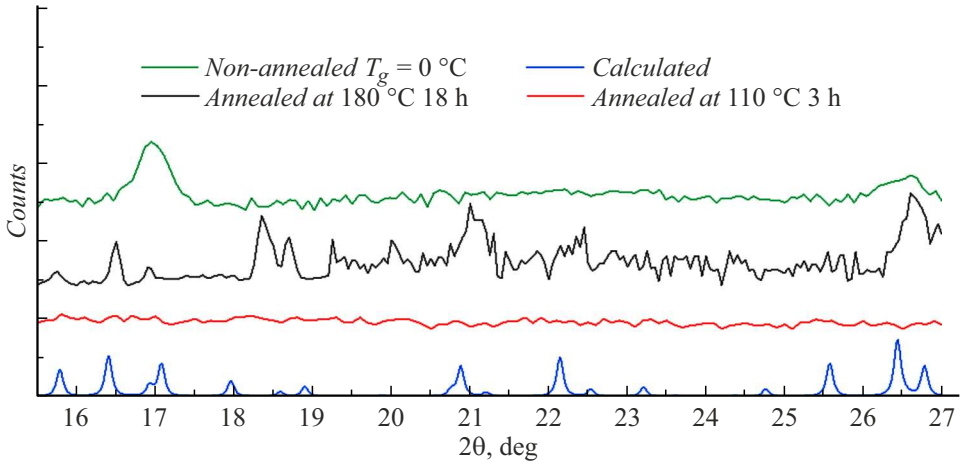

Figure 9. X-ray diffraction patterns of 100 nm SubPc films after annealing initially deposited on a silicon wafer at $T_g = 20$ °C compared with the calculated diffraction pattern and a sample grown at $T_g = 0$ °C (Figure 10).

the fact that, on the one hand, the proportion of dimers 1 decreases and, on the other hand, film crystallinity decreases (Figure 6). Identical bathochromic shift $T_g = -35$ °C was obtained in [21] after long-term annealing of SubPc film at 100 °C deposited at room temperature (RT). The authors detected a similar relief rearrangement picture and occurrence of the same reflection signal of crystal plane (002) at 17.09°. Increase in the annealing temperature will lead to even higher crystallinity growth, appearance of other reflection peaks compliant with a diffraction pattern of the initial SubPc powder (Figure 9, 10).

At 70 °C, the film becomes the least rough, consists of extended fibers reaching out from the origin of growth (Figure 2,*f*). Such SubPc film structures were studied in [16], where the authors stated that they were formed through a stacked aggregation stage into one-dimensional arrays and subsequent coalescence into large networks. It is noted [16] that such structures have anisotropy of drift mobility of charge carriers depending on whether the electric field is applied along or perpendicular to the layer surface. Films don't fully consist of stacked arrays because connection to one-dimensional structures can be made in lateral direction. Otherwise, for structures consisting only of stacked SubPc aggregates, hypsochromic shift of Q-band relative to its position in the monomer spectrum is predicted [30], which is not observed in a real film spectrum at $T_g = 70$ °C (Figure 8). Authors of [30] believe that conclusion about the stacked configuration of SubPc films made in [16] is fully erroneous and assume that one-dimensional arrays actually consist of dimers 1. However, as

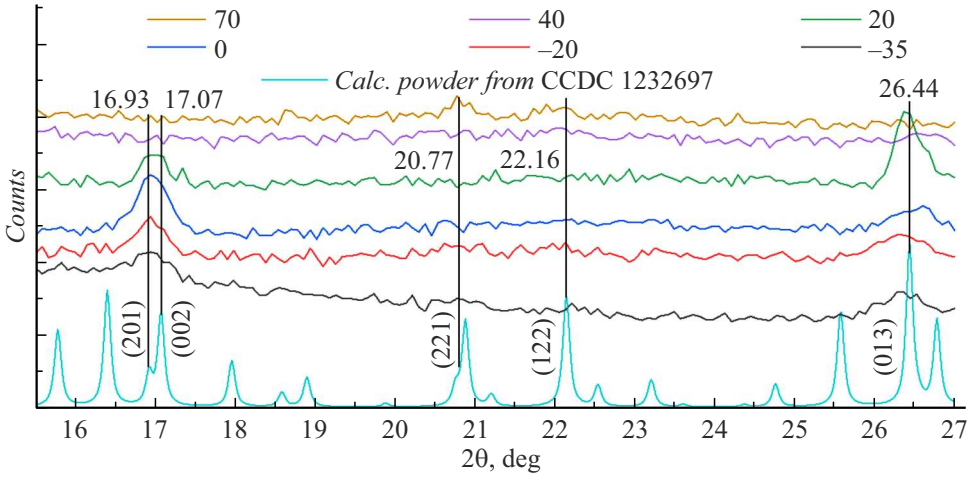

Figure 10. X-ray diffraction patterns of SubPc films deposited on silicon (100) at different temperatures, compared with the calculated powder diffraction pattern. Nominal thickness measured by X-ray reflectometry and WLI is equal to 100 nm.

Table 2. Conductivity and photoresponse of SubPc films in lateral direction between Au electrodes

T_g, °C		σ, S/m	J_{Sun}/J_{dark}
−35	Darkness	$2.30 \cdot 10^{-7}$	2.2
	Light	$6.95 \cdot 10^{-7}$	
+20	Darkness	$4.44 \cdot 10^{-8}$	10.6
	Light	$4.62 \cdot 10^{-7}$	
+70	Darkness	$3.66 \cdot 10^{-10}$	122
	Light	$4.57 \cdot 10^{-8}$	

Note. σ is the specific conductivity of films; J_{Sun}/J_{dark} is the ratio of current density in simulated sun light and in darkness at +12 B, hereinafter referred to as the photoresponse.

mentioned above, dimer 2 is theoretically more stable than dimer 1. Structural organization of one-dimensional arrays formed via SubPc deposition onto a heated substrate is still a subject of academic discussion.

As expected, films deposited at $T_g = 40\,^{\circ}\mathrm{C}$ and 70 °C, have no long-range order X-ray diffraction (Figure 6, *a*). For validation, we used the same process to deposit 100 nm, i.e. more contrast, SubPc films on silicon and measured their X-ray diffraction patterns (Figure 10). Crystallinity also disappears in them at T_g above 20 °C. Formation of amorphous uniform and flat films is a sign of reduction of the intermolecular interaction force and , therefore, of substrate affinity growth according to equation (1). However, thermodynamic and kinetic equations shown in [9,23] don't imply a change in the growth mechanism because in such narrow temperature range energies of deposited molecules γ_d and substrate surface γ_s vary insignificantly, and the deposition rate remains unchanged. A drastic change in the growth pattern, which is unlikely in these boundary conditions, has been highly likely achieved. Taking into account these optical spectra (Figure 8) and film diffraction patterns (Figures 6, 10), it becomes clear that formation of amorphous films at T_g above 40 °C, instead of SubPc monomers, involves a different particle with a different value of γ_d and substrate surface affinity γ^*, having a sufficient γ_s, highly likely the most stable type 2 dimer aggregate [30] (Figure 7). Then its diffusion length [23] will be defined by the substrate temperature (i.e. kinetically). Cases of mobile dimer and trimer particle involvement in growth processes have already occurred during deposition of inorganic films, for example, gold [23], but the question of different substrate affinity of these particles hasn't been discussed.

At intermediate values $T_g = 20\,^{\circ}\mathrm{C}-40\,^{\circ}\mathrm{C}$, uniform films, but with islands, are growing (Figure 2, *d*, *e*). Two particles likely participate simultaneously in film formation at these temperatures — SubPc monomer molecule (island growth) and „concave-to-concave" type dimer of this molecule (layer-by-layer growth). Pads, where a sublayer of SubPc molecules parallel to the substrate is still formed, can be observed in the AFM images (Figure 2, *d*, *e*) at 20 °C and 40 °C in the form of regions with raised boundaries due to more favorable growth conditions on side crystal faces (as at 0 °C).

Different proportions between molecularly-ordered domains with fast charge transport and number/width of boundaries between them, limiting the charge transfer, necessitate differences in (photo) conductivity of SubPc films. We used three key temperatures T_g — −35 °C, 20 °C and 70 °C, reflecting three types of morphology, to estimate the specific conductivity σ, [S/m], of the SubPc layer along the substrate (horizontally) between golden interdigital electrodes separated by a 30 μm gap. Measurement of horizontal conductivity for $T_g = 0\,^{\circ}\mathrm{C}$, despite the interesting structure, is obviously unreasonable — islands have virtually zero contact between them. Lateral current

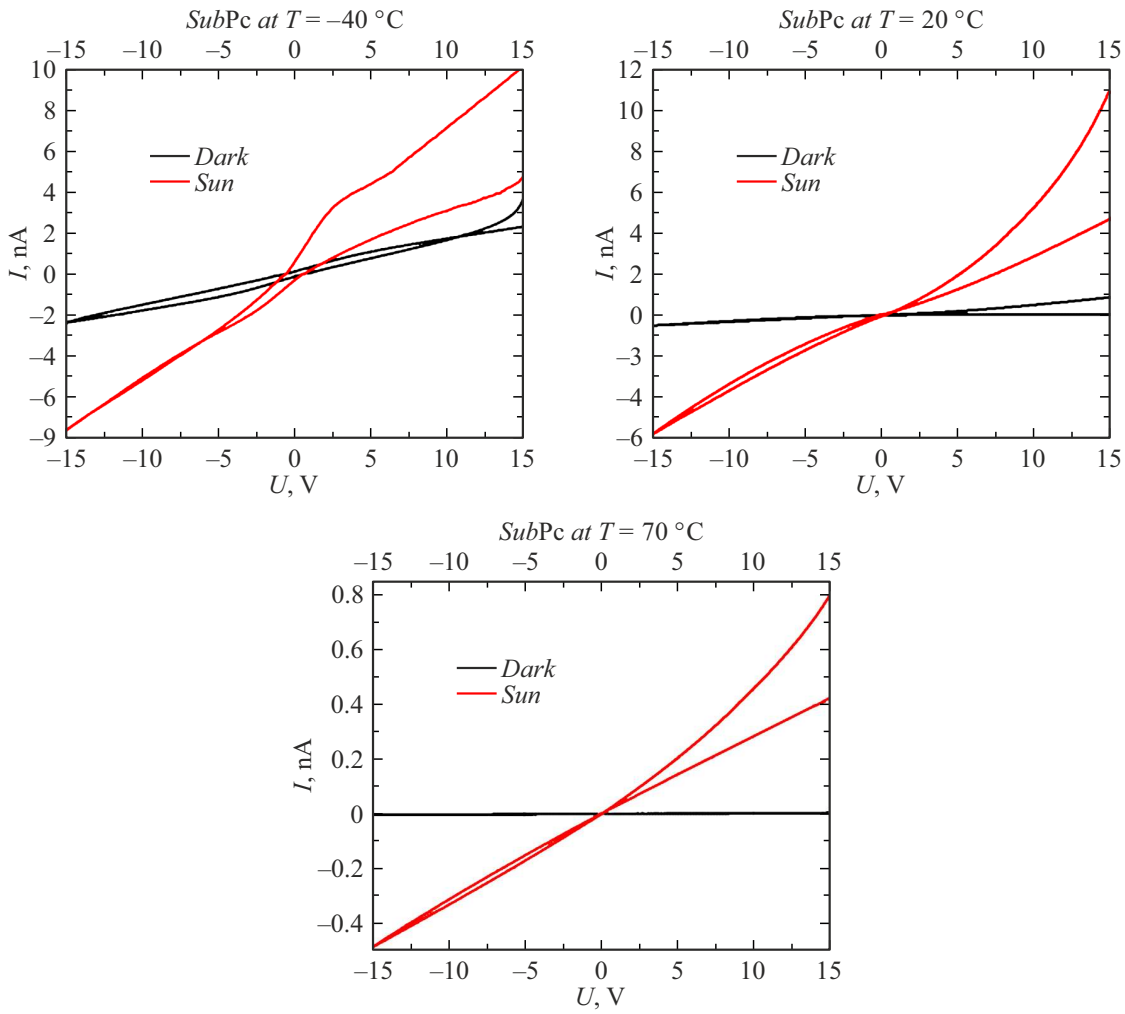

Figure 11. Current-voltage curves of 30 nm SubPc films in Au/SubPc/Au cells with interdigital electrodes. Difference of forward and reverse measurement curves is explained by capture and release of charge carriers by traps. As for phthalocyanines, hysteresis decreases as T_g grows, i.e. as the amount of traps decreases [32].

density was measured in argon in darkness and in simulated 100 mW/cm^2 sunlight.

Table 2 shows that the dark lateral conductivity σ decreases as T_g increases by three orders of magnitude; photoresponse in this case grows due to this decrease, rather than due to the photoconductivity growth. Such behavior can be possibly caused by a change in carrier trap concentration [32]. Grain boundaries obviously also serve as traps and recombination centers in SubPc films. Trap occupation and depletion affects the hysteresis range in I-V curves of Au/SubPc/Au cells (Figure 11), the lower T_g, the wider the range. Increase in the photoresponse in column-type subphthalocyanine aggregates has been already noted earlier [1].

To demonstrate the role of SubPc layer morphology in the operation of thin-film photoactive devices, ITO/Buffer/SubPc(14* nm)/C_{60}(40 nm)/BCP(8 nm)/Al(80 nm) multilayer structures were prepared, where the buffer is MoO_3, CuI, or is absent (Figure 1). The ultrathin buffer layer shall straighten the work function of the transparent ITO electrode and HOMO level of the molecular photoabsorber, thus, increasing the open-circuit voltage U_{oc} [4,12,17,20]. Only SubPc was deposited at different temperatures T_g, all other components were deposited at RT. Symbol (*) placed after the SubPc thickness serves as a reminder that this value is purely nominal considering the film relief (Figure 2, Table 1). At RT this thickness could be considered the best possible [24], but this is not applicable to films formed at other T_g [12] or deposition rates [8]. Voltage range for the I-V curve measurements was within $(+1)-(-1)$ V to ensure that the diode opening threshold voltage is overcome, but to avoid degradation of the SubPc film structure. Efficiency in the photovoltaic cell mode turned out to be low, the best value of 1.43 % was obtained at $T_g = 20\,^\circ$C, nearest to RT (Table 3), unlike 1.55 % and 1.82 % for the known cell prototypes with related structure [12,24]. Taking into account high variability of film morphology, deviation of T_g from RT just by 5 °C

Table 3. Photovoltaic properties of multilayer cells with the n-type SubPc layer

T_g	Buffer	J_{sc} (mA/cm^2)	J_{dark} (mA/cm^2)	U_{oc}, V	S	RR	FF	η, %
−35 °C	CuI	$1.3 \cdot 10^{-2}$	$7.2 \cdot 10^{-2}$	0.37	31	7	0.18	$8.9 \cdot 10^{-4}$
	MoO_3	$1.1 \cdot 10^{-3}$	$1.7 \cdot 10^{-4}$	0.6	13	0.2	0.17	$1.1 \cdot 10^{-4}$
	ITO	$9.2 \cdot 10^{-4}$	$1.2 \cdot 10^{-2}$	0.13	2	1	0.43	$5.1 \cdot 10^{-5}$
0 °C	CuI	3.2	14.1	0.49	8697	13 615	0.21	0.33
	MoO_3	$3.5 \cdot 10^{-2}$	$1.4 \cdot 10^{-1}$	0.38	1427	344	0.45	0.0065
	ITO	2.3	7.7	0.3	26 009	9253	0.34	0.24
20 °C	CuI	10	9.2	0.48	845	400	0.3	1.43
	MoO_3	2.7	3.6	0.5	5367	1440	0.17	0.24
	ITO	14.4	234	0.16	643	2127	0.32	0.75
70 °C	CuI	$7.8 \cdot 10^{-3}$	$9.6 \cdot 10^{-4}$	0.53	16	0.2	0.19	$7.7 \cdot 10^{-4}$
	MoO_3	$6.8 \cdot 10^{-3}$	$4.7 \cdot 10^{-4}$	0.64	62	0.5	0.17	$7.5 \cdot 10^{-4}$
	ITO	2	38	0.3	2709	4868	0.27	0.11

Note. J_{sc} is the current density at 0 V in sunlight; J_{dark} is the current density at +1 V in darkness; U_{oc} is the voltage, at which the generated photocurrent was fully compensated and equal to zero; S is the photoresponse calculated as a ratio of conductivity in sunlight to conductivity in darkness at −1 V; RR is the rectification calculated at a ratio of conductivity in darkness at +1 V and −1 V.

can be sufficient for the thickness of the deposited SubPc layer to go beyond the optimum thickness range because the exciton diffusion length L_D and carrier mobility μ depends greatly on SubPc layer morphology [15,16]. This can explain why the authors of [17] could get an eficiency drift of cells where SubPc was deposited at 150 °C.

In photodiode modes, the best properties $RR = 9.2 \cdot 10^3$ and $S = 2.6 \cdot 10^4$ were achieved in samples where SubPc was deposited at $T_g = 0$ °C on ITO without a CuI or MoO_3 sublayer. This cannot be attributed to the contribution of parallel-connected microscopic ITO/C_{60}/BCP/Al cells (i.e. the current bypasses SubPc) because the area of gaps in SubPc films deposited at $T_g = -35$ °C and 0 °C shall be approximately the same (Figure 2, *a*, *c*, Table 1). More likely, the successful morphology of column-type SubPc crystal domains leads to an increase in μ and L_D perpendicular to the substrate. Drift mobility μ depending on direction can differ by three orders of magnitude [16], and L_D can reach 95 nm in SubPc crystal films [15], which approximately corresponds to the height of column-type structures formed at $T_g = 0$ °C. I-V curves of multilayer cells are shown in Figure 12. As expected, introduction of the MoO_3 anode buffer increased U_{oc}, however, the impact on other photovoltaic properties was ambiguous.

The use of CuI as a buffer layer is justified for $T_g <$ RT, where films are formed by SubPc monomers. Buffer is known to have an orienting effect on phthalocyanine molecules facilitating molecule deposition parallel to the substrate [13]. In the T_g range, where the dimer aggregate is an active layer-forming particle, the use of buffer, on the contrary, leads to a significant reduction of photocurrent and all photocurrent-dependent properties of the photodiode (Table 3). Introduction of the MoO_3 layer led to an increase in serial resistance, due to which the dark current Jdark was much lower than that of CuI. Only at $T_g = 20$ °C, introduction of the layer led to a 9-fold increase in photoresponse with respect to ITO, in all other cases this layer fell short of expectations (Table 3).

Conclusions

Low-molecular boron cloride subphthalocyanine (SubPc) semiconductor layers were formed via the PVD process at different growth temperatures T_g within −35 °C− + 70 °C. It is first shown that selection of T_g in a quite narrow range allows smooth variation of the SubPc layer morphology from an island morphology on a substrate cooled below 0 °C to a uniform and homogeneous morphology on a substrate preheated to $T_g = 70$ °C. This becomes possible because the growth process likely involves two SubPc particles — monomer and dimer, which itself can be mobile already near 20 °C (RT). At 20 °C < T_g < 70 °C, film morphology is a result of joint monomer and dimer deposition, and the proportion of dimers and diffusion length are controlled thermodynamically and kinetically, respectively. According to the electronic absorption spectra and X-ray diffraction measurements, SubPc monomers form „convex-to-convex“ aggregates with molecule orientation parallel to the substrate. Multilayer diode structures with a ITO/buffer/*p*-SubPc/*n*-C_{60}/BCP/Al planar molecular heterojunction were made on the basis of SubPc layers via the PVD process. Introduction of the MoO_3 layer as a buffer leads to an increase in photovoltaic indicators of

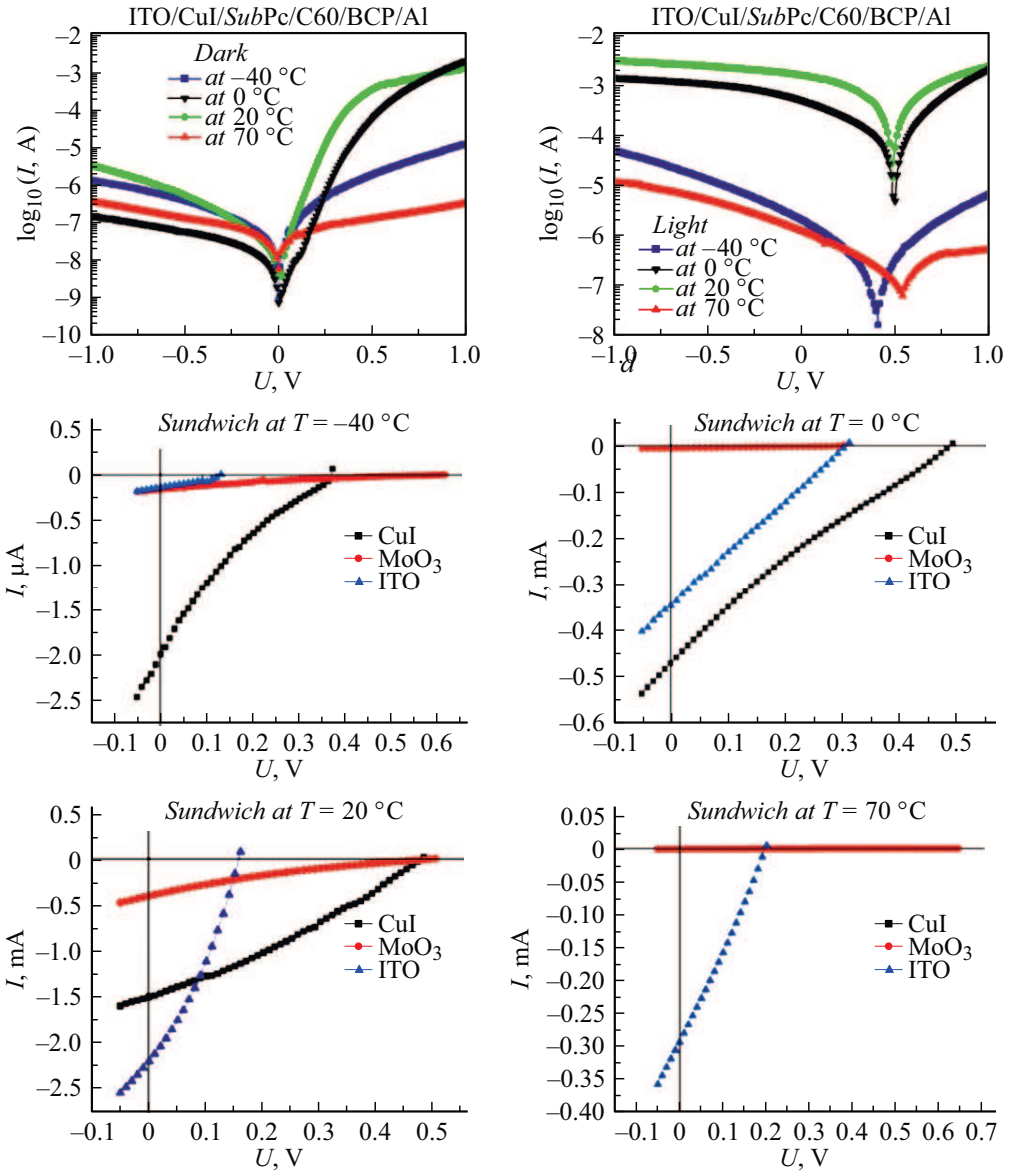

Figure 12. I-V curves of multilayer structures with the n-type SubPc layer in darkness (*a*), in simulated sunlight (*b*), selected I-V curves in quadrant IV in sunlight (*c–f*).

these structures, while CuL introduction in some cases can be reasonable. Better dark rectification and photosensitivity were achieved for structures where the SubPc layer was deposited at $T_g = 0\,^{\circ}\mathrm{C}$.

Funding

The study was supported by the Russian Science Foundation (project No. 24-23-00414).

Acknowledgments

Equipment provided by the Shared Research Facility „Physics and Technology of Micro- and Nanostructures“ of the Institute for Physics of Microstructures, Russian Academy of Sciences, was used for research activities.

The authors are grateful to Cand. Sc. (Physics and Mathematics) P.A.Yunin for useful discussions and X-ray measurements and Cand.Sc. (Chemistry) V.V.Travkin for general technical support.

Conflict of interest

The authors declare no conflict of interest.

References

[1] G. Lavarda, J. Labella, M.V. Martınez-Dıaz, M.S. Rodrıguez-Morgade, A. Osuka, T. Torres. Chem. Soc. Rev., **51** (23), 9482 (2022). DOI: 10.1039/D2CS00280A

[2] G. Akhtanova, H.P. Parkhomenko, N. Asanov, A.I. Mostovyi, N. Schopp, M. Kaikanov, V.V. Brus. Adv. Opt. Mater., **13** (24), 2501396 (2025). DOI: 10.1002/adom.202501396
[3] E. Feltri, P. Mondelli, B. Petrović, F.M. Ferrarese, A. Sharova, G. Stojanović, A. Luzio, M. Caironi. Adv. Sci., **11** (41), (2024). DOI: 10.1002/advs.202404658
[4] G.L. Pakhomov, V.V. Travkin, P.A. Stuzhin. In *Recent Advances in Boron-Containing Materials* (IntechOpen, 2020), DOI: 10.5772/intechopen.90292
[5] G.A. Nowsherwan, Q. Ali, U.F. Ali, M. Ahmad, M. Khan, S.S. Hussain. Organics, **5** (4), 520 (2024). DOI: 10.3390/org5040028
[6] J. Bisquert. J. Phys. Chem. Lett., **3** (11), 1515 (2012). DOI: 10.1021/jz300600j
[7] A.I. Koptyaev, V.V. Travkin, P.A. Yunin, K.M. Gordeev, G.L. Pakhomov. J. Mater. Sci.: Mater. Electron., **36** (17), 1053 (2025). DOI: 10.1007/s10854-025-15073-7
[8] C.-F. Lin, S.-W. Liu, C.-C. Lee, J.-C. Hunag, W.-C. Su, T.-L. Chiu, C.-T. Chen, J.-H. Lee. Sol. Energy Mater. Sol. Cells, **103**, 69 (2012). DOI: 10.1016/j.solmat.2012.04.005
[9] R.R. Cranston, B.H. Lessard. RSC Adv., **11** (35), 21716 (2021). DOI: 10.1039/D1RA03853B
[10] O. Koifman, A. Koptyaev, V. Travkin, P. Yunin, N. Somov, D. Masterov, G. Pakhomov. Colloids Interfaces, **6** (4), 77 (2022). DOI: 10.3390/colloids6040077
[11] Z.J. Comeau, R.R. Cranston, H.R. Lamontagne, C.S. Harris, A.J. Shuhendler, B.H. Lessard. Commun. Chem., **5** (1), 178 (2022). DOI: 10.1038/s42004-022-00797-y
[12] C.-T. Chou, W.-L. Tang, Y. Tai, C.-H. Lin, C.-H.J. Liu, L.-C. Chen, K.-H. Chen. Thin Solid Films, **520** (6), 2289 (2012). DOI: 10.1016/j.tsf.2011.09.062
[13] M. Li, W.-H. Li, Y.-J. Hu, J. Leng, W.-M. Tian, C.-Y. Zhao, J.-X. Liu, R.-R. Cui, S.-Y. Jin, C.-H. Cheng, S.-L. Cong. Chin. J. Chem. Phys., **35** (6), 900 (2022). DOI: 10.1063/1674-0068/cjcp2103052
[14] S.S. Harivyasi, O.T. Hofmann, N. Ilyas, O.L.A. Monti, E. Zojer. J. Phys. Chem. C, **122** (26), 14621 (2018). DOI: 10.1021/acs.jpcc.8b03675
[15] J. Wang, P. Yang, X. Zhao, L. Yang. Thin Solid Films, **636**, 527 (2017). DOI: 10.1016/j.tsf.2017.07.001
[16] S. Kalia, A. Mahajan, C.G. Ghansyam, A.K. Debnath, V. Saxsena, D.K. Aswal, R.K. Bedi. J. Appl. Phys., **121** (9), 095501 (2017). DOI: 10.1063/1.4977695
[17] Y.H. Son, G.W. Kim, W.S. Jeon, R. Pode, J.H. Kwon. Mol. Cryst. Liq. Cryst., **565** (1), 8 (2012). DOI: 10.1080/15421406.2012.690976
[18] R. Zigelstein, A.J. Lough, T.P. Bender. Acta Crystallogr. C Struct. Chem., **80** (10), 658 (2024). DOI: 10.1107/S2053229624006934
[19] G.L. Pakhomov, V.V. Travkin, A.N. Tropanova, A.I. Mashin, A.A. Logunov. Nanotechnol. Russ., **9** (1–2), 77 (2014). DOI: 10.1134/S199507801401011X
[20] P.A. Yunin, V.V. Travkin, Y.I. Sachkov, A.I. Koptyaev, P.A. Stuzhin, G.L. Pakhomov. Appl. Surf. Sci., **512**, 145645 (2020). DOI: 10.1016/j.apsusc.2020.145645
[21] C.C. Mattheus, W. Michaelis, C. Kelting, W.S. Durfee, D. Wöhrle, D. Schlettwein. Synth. Met., **146** (3), 335 (2004). DOI: 10.1016/j.synthmet.2004.08.019
[22] N.R. Gall', E.V. Rut'kov, A.Ya. Tontegode. Semiconductors, **39** (11), 1280 (2005). DOI: 10.1134/1.2128450
[23] K. Reichelt. Vacuum, **38** (12), 1083 (1988). DOI: 10.1016/0042-207X(88)90004-8
[24] J. Kim, S. Yim. Appl. Phys. Lett., **99** (19), (2011). DOI: 10.1063/1.3660710
[25] T. Mirabito, B. Huet, J.M. Redwing, D.W. Snyder. ACS Omega, **6** (31), 20598 (2021). DOI: 10.1021/acsomega.1c02758
[26] S. Tabuchi, Y. Otsuka, M. Kanai, H. Tabata, T. Matsumoto, T. Kawai. Org. Electron., **11** (5), 916 (2010). DOI: 10.1016/j.orgel.2010.02.011
[27] G.L. Pakhomov, A.I. Koptyaev, P.A. Yunin, N.V. Somov, A.S. Semeikin, E.D. Rychikhina, P.A. Stuzhin. Chem. Select, **8** (45), e202303271 (2023). DOI: 10.1002/slct.202303271
[28] M. Trelka, A. Medina, D. Écija, C. Urban, O. Gröning, R. Fasel, J.M. Gallego, C.G. Claessens, R. Otero, T. Torres, R. Mirandaae. Chem. Commun., **47** (36), 9986 (2011). DOI: 10.1039/c1cc11658d
[29] K.L. Sampson, X. Jiang, E. Bukuroshi, A. Dovijarski, H. Raboui, T.P. Bender, K.M. Kadish. J. Phys. Chem. A, **122** (18), 4414 (2018). DOI: 10.1021/acs.jpca.8b02023
[30] X. Chen, S Zheng. Org. Electron., **62**, 667 (2018). DOI: 10.1016/j.orgel.2018.07.005
[31] J. Zhang, Y. Li, X. Jiang, Z. Wang, C. Yang. Dyes Pigm., **170**, 107584 (2019). DOI: 10.1016/j.dyepig.2019.107584
[32] V. Rani, A. Sharma, P. Kumar, B. Singh, S. Ghosh. RSC Adv., **7** (86), 54911 (2017). DOI: 10.1039/C7RA08316E

Translated by E.Ilyinskaya